BULLETIN OF THE POLISH ACADEMY OF SCIENCES
TECHNICAL SCIENCES, Vol. 62, No. 2, 2014
DOI: 10.2478/bpasts-2014-0038

VARIA

Selected aspects of Modular Multilevel Converter operation

M. ZYGMANOWSKI[1], B. GRZESIK[1], M. FULCZYK[2], and R. NALEPA[2*]

[1] Department of Power Electronics, Electrical Drives and Robotics, Silesian University of Technology, 2B Krzywoustego St., 44-100 Gliwice, Poland

[2] ABB Sp. z o.o., Corporate Research Centre, 13A Starowislna St., 31-038 Krakow, Poland

Abstract. The operation of the Modular Multilevel Converter (MMC) is the main subject of this paper. Selected operation aspects are discussed on the basis of the averaged model, with a special focus on power section parameters and control. The direct modulation method has been chosen for the control of the MMC.

Key words: Modular Multilevel Converter MMC, power electronic converter modeling.

Nomenclature

In this paper the following symbols are adopted for description of the modular multilevel converter operation and its parameters:

C_{arm}	–	arm capacitance,
C_{SM}	–	submodule capacitance,
E_{V}	–	amplitude of fundamental component of output voltage e_{V},
e_{V}	–	output voltage related to converter medium point of dc-link,
$E_{\text{V,max}}$	–	maximum value of the output voltage,
f_{m}	–	fundamental frequency,
i_{armU}, i_{armL}	–	upper (U) and lower (L) arm currents,
i_{cc}	–	circulating current, being a part of the difference current i_{diff},
i_{CU}, i_{CL}	–	submodule capacitor current,
i_{dc}	–	Dc-link current,
$I_{\text{dc,ac}}$	–	alternating component of the dc-link current,
$I_{\text{dc,AV}}$	–	average value of the dc-link current,
i_{diff}	–	difference current, $i_{\text{diff}} = (i_{\text{armU}} + i_{\text{armL}})/2$,
$i_{\text{diff,ac}}$	–	alternating component of the difference current i_{diff} (the rms value of which is $I_{\text{diff,ac,RMS}}$),
$I_{\text{diff,dc}}$	–	Dc component of the difference current i_{diff},
I_{V}	–	amplitude of the output current i_{V} fundamental component,
i_{V}	–	output current,
L_{arm}	–	arm inductance,
m_{a}	–	modulation index,
n	–	number of submodules in converter arm,
n_{U}, n_{L}	–	modulating signals in upper and lower arms,
R_{arm}	–	arm resistance,
R_{ESR}	–	equivalent series resistance of a single submodule capacitor,
r_{on}	–	average on-state resistance of a single switch,
r_{pU}, r_{pL}	–	non-ideal parameter arm resistances,
r_{T}, r_{D}	–	on-state resistance of single transistor and diode,
S_{NU}, S_{NL}	–	carrier signals for upper and lower arm,
T_{PWM}	–	switching period, $T_{\text{PWM}} = 1/f_{\text{PWM}}$,
V_{dc}	–	rated value of dc-link voltage,
v_{dc}	–	Dc-link voltage,
v_{disU}, v_{disL}	–	discrepancy arm voltage components,
v_{pU}, v_{pL}	–	non-ideal parameter arm voltages,
V_{T0}, V_{D0}	–	on-state threshold voltage of a single transistor and diode,
$v_{\text{CU}k}$, $v_{\text{CL}k}$	–	k submodule capacitor voltage in the upper (U) and lower arm (L),
v_{CU}, v_{CL}	–	arm capacitor voltage – the sum of n capacitor voltages in the upper (U) and lower arm (L),
v_{armU}, v_{armL}	–	upper and lower arm voltages,
$v_{arm,\text{max}}$	–	maximum value of arm voltage,
γ	–	phase angle between carriers signals S_{NU} and S_{NL},
ΔV_{C}	–	peak-to-peak value of voltage ripple in a sum of voltages across capacitors in a single arm,
$\Delta i_{\text{diff,max}}$	–	maximum difference current ripple,
φ	–	output phase-shift angle,
ψ	–	phase angle of modulating signals in phase A,
ω	–	angular frequency, $\omega = 2\pi f_{\text{m}}$.

*e-mail: marcin.zygmanowski@polsl.pl

1. Introduction

The modular multilevel converter (MMC) is one of the newest and most promising power electronic converters intended for very and ultra high voltage and power applications, particularly for HVDC systems [1, 2]. The converter converts electrical energy from ac voltage to dc voltage or from dc voltage to ac voltage. Its specific topology, without the need for the dc-link capacitor bank, and full modularity, make it suitable also for medium voltage applications, e.g. medium voltage electric drives [3, 4]. Such a wide range of application fields for a single topology makes it challenging to understand all important circuit selection and operation aspects. The challenge does not disappear even if advanced numerical circuit simulations are deployed – simulation is not a substitute for sufficient understanding of this advanced circuit.

The topology relies on the well-known half-bridge (or full-bridge) switching cell with a capacitor inside – called in this paper "SubModule", SM. SMs can be connected in series to satisfy application voltage requirements. SMs connected in this way, under a certain control scheme, turn into a technology enabler for high voltage power electronic circuits.

One of the most popular topologies with SMs can be seen in Fig. 1. In this circuit the capacitors of SMs are subject to voltages ($v_{\mathrm{CU}XY}$, $v_{\mathrm{CL}XY}$). Here, $X = A, B$ or C, $Y = 1, 2, ...n$, where n is the number of SMs in each converter arm. Two arms – an upper (U), and a lower arm (L) are connected in series and constitute one converter phase.

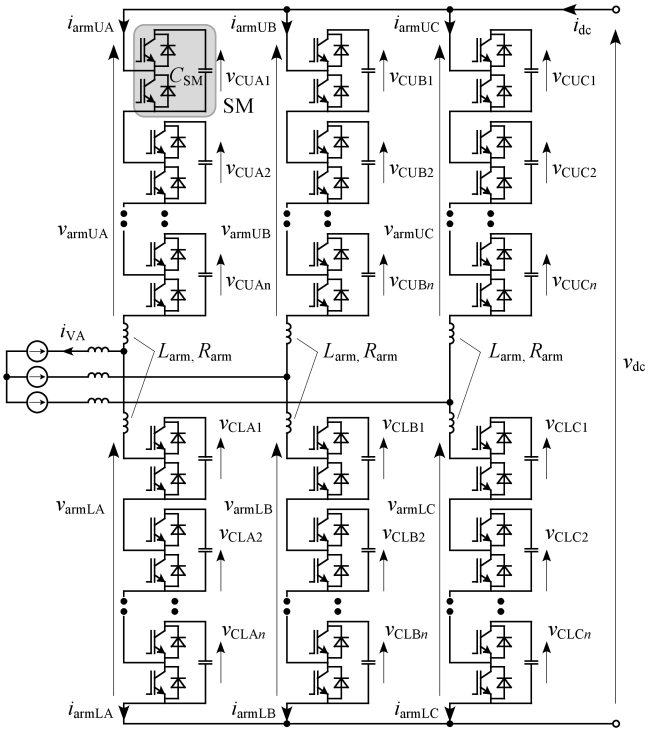

Fig. 1. Three-phase modular multilevel converter, connected to the grid, with n submodules SM in each converter arm

In this paper the MMC operation is explained by means of state equations. The equations have been derived on the basis of an averaged model for each converter phase [2] – they have led to a mathematical, linear but time-varying model of the MMC. Using this model, the MMC operation is explained on the basis of a system configuration example. Furthermore, the submodule capacitor voltage ripple is discussed together with currents circulating inside the MMC. These currents are named circulating currents, and are parts of a difference current which flows through both arms of each converter phase.

The second MMC model presented in the paper is a detailed simulation model, which allows verifying the correctness of results obtained for the averaged model.

The MMC control method has an impact on the converter operation and its components selection, not only the capacitor C_{SM} [5], but also the arm resistance R_{arm} (as a resultant design value rather than a design parameter) and the inductance L_{arm} [5, 6]. For the purpose of this article, the direct modulation method [7, 8] is assumed to be used in both MMC models. In this method transistors in submodules are switched according to sinusoidal modulating signals, without any feedback from capacitor voltages.

2. Averaged model of MMC

The averaged model of the three-phase MMC (Fig. 2) is based on the approach that output arm voltages $v_{\mathrm{armU}X}$ and $v_{\mathrm{armL}X}$ are continuous rather than switched in the PWM manner. An analysis of the converter operation can be performed for each phase separately, and phase denotations ($X = A, B$ or C) for all values are omitted for the sake of simplicity. This is possible due to the assumption that the dc-link circuit is ideal and modelled as a dc voltage source.

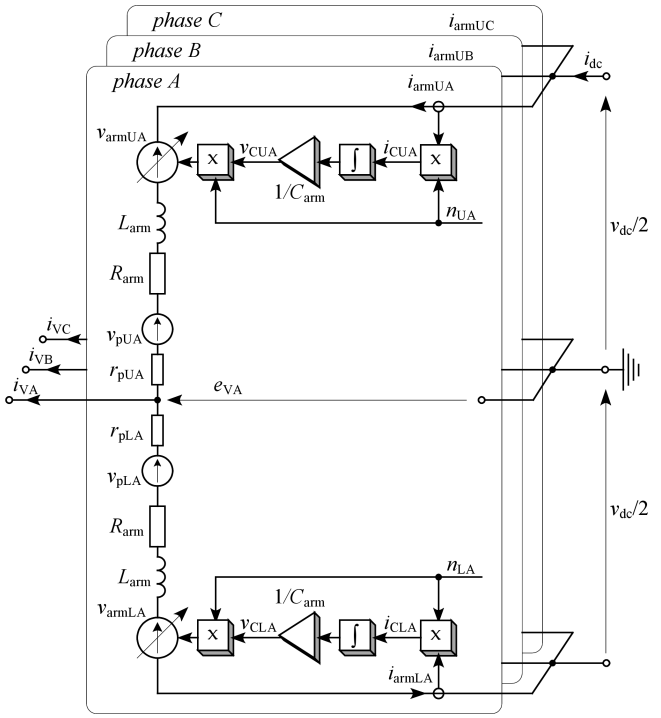

Fig. 2. Three-phase modular multilevel converter averaged model with arm voltage controlled sources as per Eqs. (1)–(3)

Converter arm voltages are

$$v_{\text{armU}} = n_{\text{U}} v_{\text{CU}}, \qquad v_{\text{armL}} = n_{\text{L}} v_{\text{CL}}, \tag{1}$$

where n_{U} and n_{L} are the normalized modulating signals raging from 0 (corresponding to the state when all arm submodules are turned off) to 1 (when all submodules in the converter arm are turned on). Upper and lower arm voltages (v_{CU}, v_{CL}) are sums of adequate n-capacitors voltages, (2).

$$v_{\text{CU}} = \sum_{k=1}^{n} v_{\text{CU}k}, \qquad v_{\text{CL}} = \sum_{k=1}^{n} v_{\text{CL}k}. \tag{2}$$

In the converter averaged model all submodules in one arm can be replaced by controlled voltage sources according to (1).

This replacement alone is not sufficient because the arm voltages v_{armU} and v_{armL} are built up of the capacitor voltages $v_{\text{CU}k}$ and $v_{\text{CL}k}$. Thus, it is necessary for each converter arm to include a modulated capacitance, which can operate according to (3), as presented in Fig. 2.

$$i_{\text{armU}} = \frac{C_{\text{arm}}}{n_{\text{U}}} \frac{\text{d}v_{\text{CU}}}{\text{d}t}, \qquad i_{\text{armL}} = \frac{C_{\text{arm}}}{n_{\text{L}}} \frac{\text{d}v_{\text{CL}}}{\text{d}t}, \tag{3}$$

where C_{arm} is the capacitance of the series connection of all n arm submodule capacitances, $C_{\text{arm}} = C_{\text{SM}}/n$; i_{armU} and i_{armL} are upper and lower arm currents respectively. Both Eqs. (3) are state equations, describing the dynamics of the converter. With the modulated capacitances the MMC can be simplified to the form presented in Fig. 2.

In accordance with the Kirchhoff voltage law, two equations can be written:

$$\begin{aligned} \frac{V_{\text{dc}}}{2} &= R_{\text{arm}} i_{\text{armU}} + L_{\text{arm}} \frac{\text{d}}{\text{d}t}\left(i_{\text{armU}}\right) + v_{\text{armU}} + e_{\text{V}}, \\ \frac{V_{\text{dc}}}{2} &= R_{\text{arm}} i_{\text{armL}} + L_{\text{arm}} \frac{\text{d}}{\text{d}t}\left(i_{\text{armL}}\right) + v_{\text{armL}} - e_{\text{V}}. \end{aligned} \tag{4}$$

Summing up both Eqs. (4) leads to a third state equation as follows:

$$\frac{\text{d}}{\text{d}t} i_{\text{diff}} = -\frac{R_{\text{arm}}}{L_{\text{arm}}} i_{\text{diff}} - \frac{v_{\text{armU}} + v_{\text{armL}}}{2L_{\text{arm}}} + \frac{V_{\text{dc}}}{2L_{\text{arm}}}, \tag{5}$$

where i_{diff} can be calculated as half of a sum of arm currents, $i_{\text{diff}} = (i_{\text{armU}} + i_{\text{armL}})/2$. The i_{diff} is the arm current component, which is the same in both converter arms and can be written as:

$$i_{\text{armU}} = \frac{i_{\text{V}}}{2} + i_{\text{diff}}, \qquad i_{\text{armL}} = -\frac{i_{\text{V}}}{2} + i_{\text{diff}}, \tag{6}$$

where i_{V} is the converter output current as in Fig. 2.

Defining the i_{diff} reduces the number of the state variables down to 3 per each converter phase. The Eqs. (3), (5) and (6) can be written as

$$\begin{aligned} \frac{\text{d}}{\text{d}t} \begin{bmatrix} i_{\text{diff}} \\ v_{\text{CU}} \\ v_{\text{CL}} \end{bmatrix} &= \begin{bmatrix} -\frac{R_{\text{arm}}}{L_{\text{arm}}} & -\frac{n_{\text{U}}}{2L_{\text{arm}}} & -\frac{n_{\text{L}}}{2L_{\text{arm}}} \\ \frac{n_{\text{U}}}{C_{\text{arm}}} & 0 & 0 \\ \frac{n_{\text{L}}}{C_{\text{arm}}} & 0 & 0 \end{bmatrix} \\ &\cdot \begin{bmatrix} i_{\text{diff}} \\ v_{\text{CU}} \\ v_{\text{CL}} \end{bmatrix} + \begin{bmatrix} \frac{V_{\text{dc}}}{2L_{\text{arm}}} \\ \frac{n_{\text{U}} i_{\text{V}}}{2C_{\text{arm}}} \\ -\frac{n_{\text{L}} i_{\text{V}}}{2C_{\text{arm}}} \end{bmatrix}. \end{aligned} \tag{7}$$

Equation (7) is linear and time-variant because the state matrix has four coefficients n_{U} and n_{L}, which both are time-varying. To find out the exact form of the modulation signals n_{U} and n_{L}, Eq. (4) are subtracted from each other to give the output voltage e_{V} (8)

$$e_{\text{V}} = \frac{v_{\text{armL}} - v_{\text{armU}}}{2} - \frac{R_{\text{arm}}}{2} i_{\text{V}} - \frac{L_{\text{arm}}}{2} \frac{\text{d}i_{\text{V}}}{\text{d}t}, \tag{8}$$

here according to (6) $i_{\text{armU}} - i_{\text{armL}} = i_{\text{V}}$. Assuming that voltage drops across R_{arm} and L_{arm} are smaller than v_{armL} and v_{armU}, the output voltage can be simplified to

$$e_{\text{V}} \approx \frac{v_{\text{armL}} - v_{\text{armU}}}{2}. \tag{9}$$

Assuming that $e_{\text{V}} = E_V \sin(\omega t)$ and $v_{\text{armL}} + v_{\text{armU}} = V_{\text{dc}}$, the arm voltages, generated by submodules, have to fulfil the following equations:

$$\begin{aligned} v_{\text{armU}} &= \frac{V_{\text{dc}}}{2} - E_{\text{V}} \sin\left(\omega t - \psi\right), \\ v_{\text{armL}} &= \frac{V_{\text{dc}}}{2} + E_{\text{V}} \sin\left(\omega t - \psi\right). \end{aligned} \tag{10}$$

Due to the fact that the arm voltages are positive ($v_{\text{armL}} > 0$, $v_{\text{armU}} > 0$), the maximum value of the output voltage is $E_{\text{V,max}} = V_{\text{dc}}/2$. This assumption also allows determining the maximum arm voltage.

$$v_{\text{armU,max}} = v_{\text{armL,max}} = \frac{V_{\text{dc}}}{2} + E_{\text{V,max}} = V_{\text{dc}}. \tag{11}$$

From (11) one can see that, due to the maximum value of the modulating signals equal to one, $n_{\text{U,max}} = n_{\text{L,max}} = 1$, the sum of capacitor voltages in each arm should be set at

$$v_{\text{CU,AV}} = v_{\text{CL,AV}} = V_{\text{dc}}. \tag{12}$$

Modulating signals n_{U} and n_{L} are determined from (10) according to (13)

$$\begin{aligned} n_{\text{U}} &= \frac{v_{\text{armU}}}{V_{\text{dc}}} = \frac{1 - m_{\text{a}} \sin\left(\omega t - \psi\right)}{2}, \\ n_{\text{L}} &= \frac{v_{\text{armL}}}{V_{\text{dc}}} = \frac{1 + m_{\text{a}} \sin\left(\omega t - \psi\right)}{2}, \end{aligned} \tag{13}$$

where m_{a} is the modulation index and its value is between 0 and 1. Equations (13) represent the direct modulation method used for controlling the MMC. In the converter analysis presented in this paper the modulating signals n_{U} and n_{L} are without the third harmonic injection.

Difference current. Assuming that the sums of capacitor voltages are constant at a given V_{dc}, $v_{\text{CU}} = v_{\text{CL}} = V_{\text{dc}}$, the modulating signals, n_{U} and n_{L}, are as per (13), and from Kirchhoff voltage law $v_{\text{armU}} + v_{\text{armL}} = V_{\text{dc}}$, the derivative of the difference current (5) is equal to (14).

$$\frac{\text{d}}{\text{d}t} i_{\text{diff}} = -\frac{R_{\text{arm}}}{L_{\text{arm}}} i_{\text{diff}}. \tag{14}$$

The solution to this equation is non-periodic – as is expected for the converter operating in the steady state. It means that the assumption $v_{\text{armU}} + v_{\text{armL}} = V_{\text{dc}}$ is no longer valid,

and when modulating signals n_U and n_L are given as (13), the sums of capacitor voltages deviate from their rated values. In other words – the capacitor voltage ripple always exists in the MMC, as per (3). The issue of the capacitor voltage ripple is investigated later in this paper.

Capacitor voltage ripple together with other non-ideal parameters of the MMC (represented by voltage sources v_{pU} and v_{pL}) causes difference current oscillations. In the best case the difference current is constant and equals to 1/3 of the dc current i_{dc}. Achieving this best case state is the aim of the MMC control method known as open-loop control [7, 9] and other control methods [10, 11]. Reducing the difference current to merely the dc component minimizes MMC power losses [12]. On the other hand, allowing the difference current oscillation simplifies the MMC control. A compromise based on the understanding of the MMC nature is highly recommended at this point. The difference current i_{diff}, can be divided into two components. The first one equals $1/3 i_{dc}$ and the second one is the circulating current as in (15):

$$i_{diff} = \frac{i_{dc}}{3} + i_{cc} = \frac{I_{dc,AV}}{3} + \frac{i_{dc,ac}}{3} + i_{cc} = I_{diff,dc} + i_{diff,ac}. \quad (15)$$

The circulating current i_{cc} flows between MMC phases and is composed of negative and positive sequence components (excluding fundamental and zero-sequence components). Typically the second harmonic is a dominant part of the circulating current. The i_{dc} is composed of a dc component $I_{dc,AV}$, delivering the active power from/to the dc circuit, and of an alternating component $i_{dc,ac}$, which consists of zero-sequence components (harmonics multiples of the third harmonic e.g. sixth).

The sum of non-constant components of the difference current, $i_{dc,ac}/3 + i_{cc} = i_{diff,ac}$ is an ac component which generates extra power losses in the MMC – without transmission of the effective power between the ac side and dc circuit. The ac component of the difference current, $i_{diff,ac}$, is minimized (ideally down to zero) by the open loop control method [3, 7] – as opposed to the MMC operating under the direct modulation method governed by (13), where the $i_{diff,ac}$ can be large.

Capacitor voltage ripple. When the direct modulation method is applied, the capacitor voltage ripple can be evaluated by using the averaged MMC model described by Eqs. (1)–(13). The peak-to-peak value of the capacitor voltage, ΔV_C is treated as a design criterion in this paper.

Capacitor voltage ripple, ΔV_C, depends on the capacitor currents i_{CU} and i_{CL}, which depend on the modulation signals n_U and n_L and the arm currents i_{armU} and i_{armL} according to:

$$i_{CU} = n_U i_{armU}, \qquad i_{CL} = n_L i_{armL}. \quad (16)$$

Arm currents i_{armU} and i_{armL} in the MMC operating under the direct modulation control consist of circulating current i_{cc} [13] which, together with other components of the arm currents, influences capacitor voltage ripples. Moreover these voltage ripples directly influence circulating currents. The results presented in the next section are obtained by using simulations of the averaged model of single-phase converter in Matlab/Simulink. Similar results have been obtained in a model developed in GeckoCIRCUITS.

3. Selection of the MMC parameters

In this section the operation of the converter is presented for selected parameters collated in Table 1. With such parameters and the assumption that output currents are sinusoidal as in (17), the selected waveforms for phase A are shown in Fig. 3.

$$i_{VA} = I_V \sin(\omega t - \psi - \varphi),$$
$$i_{VB} = I_V \sin(\omega t - \psi - \varphi - 2\pi/3). \quad (17)$$

Table 1
Parameters of the MMC simulation model

Name of the parameter	Symbol	Value
DC circuit voltage	V_{dc}	5 kV
output current amplitude	I_V	40 A
angular frequency	ω	314.15 rad/s
phase angle	φ	0 deg
modulating signal phase angle	ψ	0 deg
modulation index	m_a	1
arm inductance	L_{arm}	750 μH
arm resistance	R_{arm}	100 Ω
arm capacitance	C_{arm}	50 μF

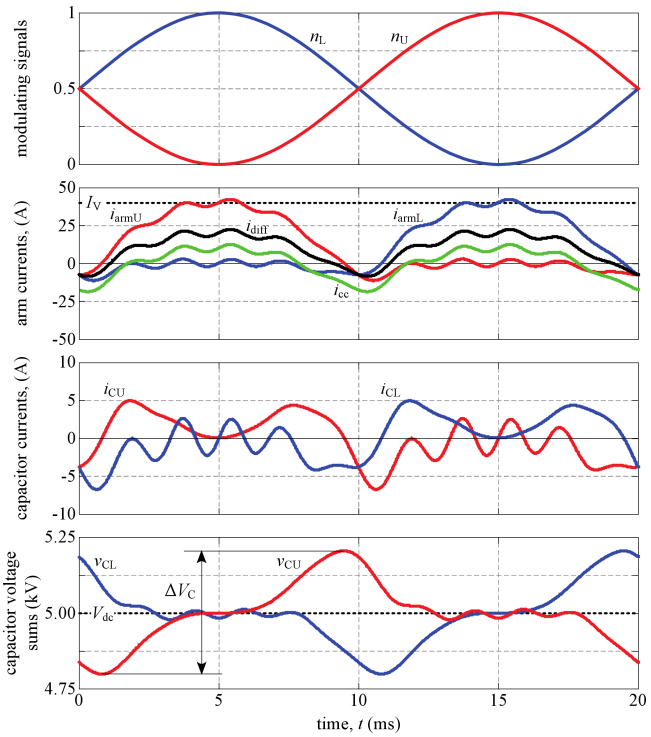

Fig. 3. Waveforms of the MMC averaged model operating with the direct modulation control method – parameters are given in Table 1

Figure 3 presents the waveforms of modulating signals n_U and n_L (13); arm currents, i_{armU}, i_{armL}, with their components as per (6) and (15); capacitor currents, i_{CU}, i_{CL} (as in (16)); and the peak-to-peak value, ΔV_C, of the capacitor voltage sums, v_{CU}, v_{CL}. The rms value of the difference current ac

component, and the peak-to-peak value of the capacitor voltage are considered in this paper as a criterion for selecting the arm capacitances C_{arm} – in the presence of changing arm resistance R_{arm}. The arm inductance for the purpose of this paper has been set at $L_{\text{arm}} = 0.75$ mH.

The first analysis concerns the influence of the R_{arm} on the rms value of the ac component of the difference current, $I_{\text{diff,ac,RMS}}$, see Fig. 4. It can be seen in this figure that a larger R_{arm} gives a smaller $I_{\text{diff,ac,RMS}}$. Exemplary characteristics of the current $I_{\text{diff,ac,RMS}}$ are presented for capacitance C_{arm} raging from 0.05 mF to 1 mF – equivalent to $C_{\text{SM}} = n{\times}0.05$ mF and $n{\times}1$ mF in n-submodule converter. Such capacitances in the three-phase converter correspond to the energy-to-power ratio raging from 25 J/kW to 500 J/kW, where the converter rated power is calculated from $P = (3/2)m_a E_{\text{V}} I_{\text{V}} = 150$ kW, which is obtained for parameters from Table 1 and the amplitude of the phase voltage $E_{\text{V}} = V_{\text{dc}}/2$. In practice a lower energy-to-power ratio decreases the cost of the converter. However, for the generality of the analysis presented in this paper higher energy-to-power ratios are considered.

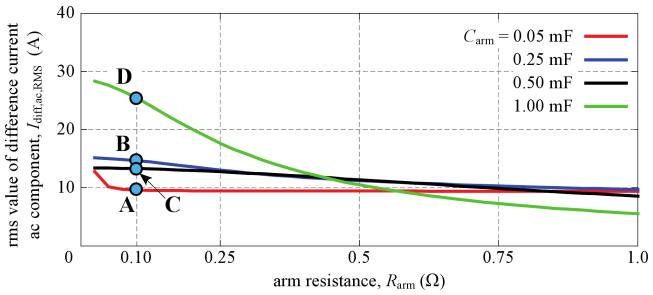

Fig. 4. The rms values of the difference current AC component, $I_{\text{diff,ac,RMS}}$ as a function of R_{arm} parameterized with C_{arm}

As can be seen in Fig. 4 the influence of the arm capacitances on the difference current ac component $I_{\text{diff,ac,RMS}}$ is nonmonotonic. It is discussed later in this paper as an effect of resonances between L_{arm} and modulated C_{arm} – mostly at second and fourth harmonics [5, 13]. During the selection of the MMC components these resonances should be taken into consideration.

Harmonic spectra of the $i_{\text{diff,ac}}$ for the MMC with different capacitances, which correspond to points A-D in Fig. 4, are presented in Fig. 5. In the case of point A, corresponding to parameters given in Table 1, the even harmonics exist – with a dominant second harmonic. At point B, both second and fourth harmonics are explicit.

Selection of arm capacitance C_{arm} demands a similar analysis to the $i_{\text{diff,ac}}$ assessment in the function of arm resistance R_{arm}. In Fig. 6 the results of such an analysis are presented for four different values of R_{arm}.

Resonances in circulating current occur for the fixed value of $L_{\text{arm}} = 0.75$ mH, with different values of C_{arm} [5, 13]. This confirms that the mathematical description of the converter operating under direct modulation is quite complex. In Fig. 6 four distinguished points (A-D) are selected, for which harmonic spectra are given in Fig. 7.

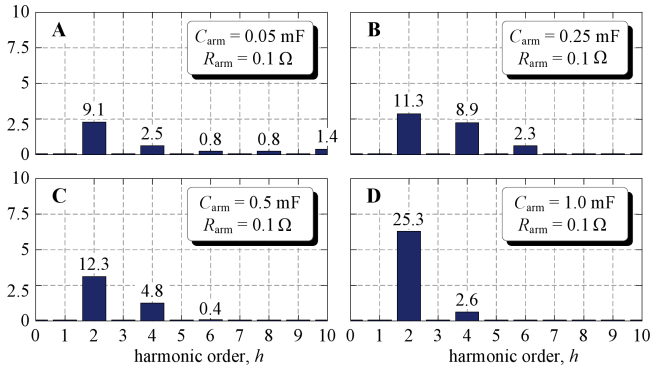

Fig. 5. Harmonic spectra (rms values in amperes) of the difference current alternating component $i_{\text{diff,ac}}$ at points A-D (as per Fig. 4)

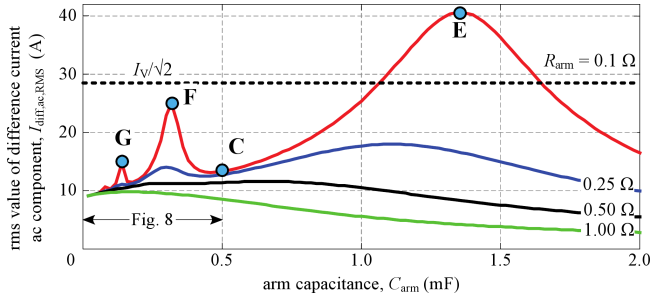

Fig. 6. The rms values of the difference current AC component, $I_{\text{diff,ac,RMS}}$ as a function of C_{arm} parameterized with R_{arm}

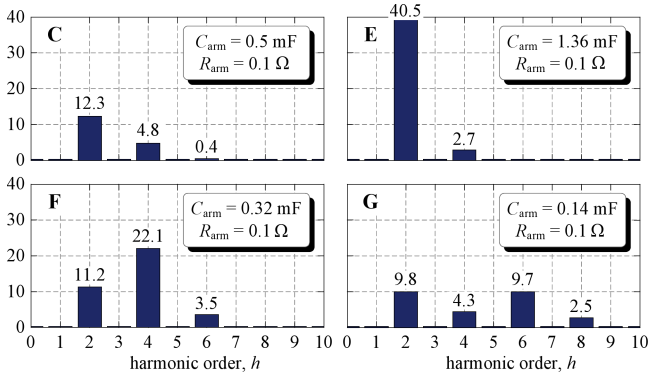

Fig. 7. Harmonic content (rms values in amperes) of the difference current AC component $i_{\text{diff,ac}}$ at points B and E-G (as in Fig. 6)

At point E resonance at the second harmonic exists, at point F resonance occurs at fourth harmonic. Point C lies between points E and F. At point G another resonance occurs having distributed spectrum among second and sixth harmonics, with smaller fourth and eighth. In a three-phase converter the sixth harmonic in the difference current is a zero-sequence component and flows through the dc circuit (observed in i_{dc}) while the other harmonics (positive and negative-sequence) close through the MMC phases (as circulating current i_{cc}).

Resonances occurring in the difference current are much more evident in Fig. 8, which presents the same characteristics as in Fig. 6 but for smaller arm capacitances C_{arm}. Arm capacitances smaller than 0.1 mF ($C_{\text{arm}} < 0.1$ mF) allow avoiding resonances at small order harmonics (2^{nd}, 4^{th} and 6^{th}). It should be noted that such arm capacitance C_{arm} results from the resonance with arm inductance and for other values of L_{arm} the results can be different. In summary, it can be concluded that arm capacitance C_{arm} should be determined together with other converter parameters. Possible resonances have to be taken into consideration.

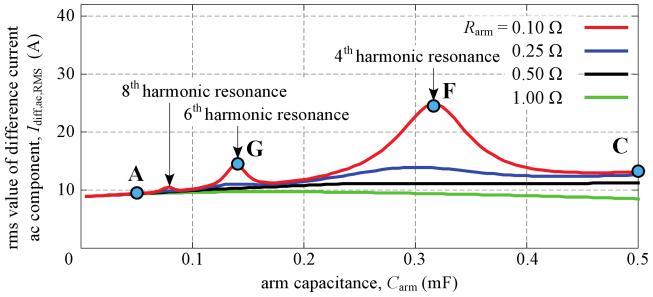

Fig. 8. The rms values of the difference current AC component, $I_{\text{diff,ac,RMS}}$ as a function of C_{arm} parameterized with R_{arm} with indicated resonances of fourth, sixth and eighth harmonics

Another criterion for arm capacitance selection is arm capacitor voltage ripple, ΔV_{C}. Here, in the converter averaged model the ΔV_{C} is defined as a peak-to-peak value of ripples observed in sums of capacitor voltages v_{CU} or v_{CL}. For a single submodule capacitor the voltage ripple is n times smaller than ΔV_{C}. This is because of the assumption that all capacitor voltages inside a particular converter arm are equal due to the balancing operation of a submodule selector [1]. Analyses of the capacitor voltage ripples have been performed for the same MMC parameters as in the previous case, except the phase angle φ, which is changing or set to 80° or 0°. The first value ($\varphi = 80°$) has been dictated by the largest voltage ripple $\Delta V_{\text{C}} = 623$ V (Fig. 9 – point H). Point A in Fig. 9 corresponds to the ripple ΔV_{C} shown in Fig. 3, where $\Delta V_{\text{C}} = 406$ V. This means that the largest voltage ripples, for the converter operating with parameters given in Table 1, are below $13\% V_{\text{dc}} = 650$ V. In many publications, [8, 14], authors report even larger values of voltage ripples e.g. 20% V_{dc}.

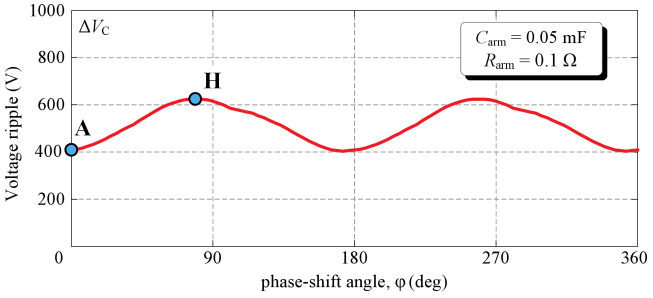

Fig. 9. Arm capacitor voltage ripple ΔV_{C} as a function of phase-shift angle φ

In Fig. 10 arm capacitor voltage ripple ΔV_{C} is shown as a function of arm capacitance C_{arm}. From this figure it can be seen that resonances still influence voltage ripple ΔV_{C}.

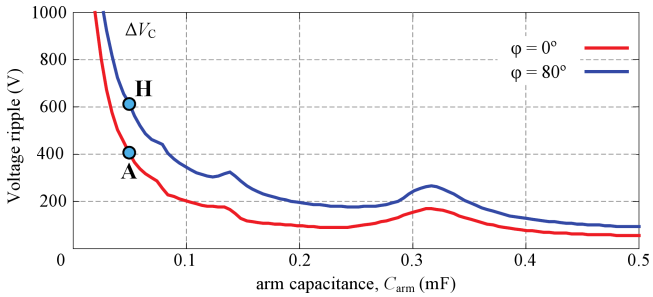

Fig. 10. Arm capacitor voltage ripple ΔV_{C} as a function of C_{arm}

The influence of arm resistance R_{arm} on arm capacitor voltage ripple ΔV_{C} is presented in Fig. 11. This ripple is nearly constant for a wide range of R_{arm}.

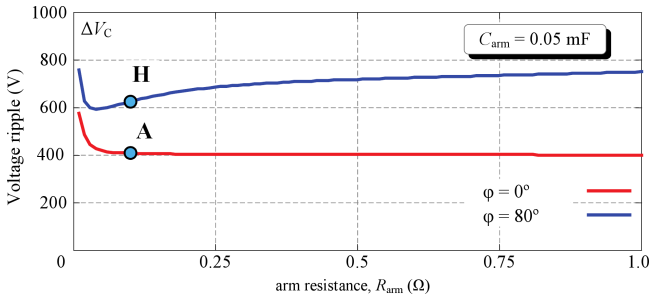

Fig. 11. Arm capacitor voltage ripple ΔV_{C} as a function of R_{arm}

Similarly to the analysis of the circulating current, the arm capacitor voltage ripple ΔV_{C} analysis shows that the parameter selection for modular multilevel converter is a multidimensional optimization problem. The presented results show the general behaviour of the converter with partially selected parameters. During the converter design process some aspects presented in this section can be useful. It should be noted that for different converter parameters the achieved results can be slightly different.

4. Influence of non-ideal parameters on MMC operation

The transistor and diode on-state resistances, capacitor series equivalent resistances, threshold on-state voltages in switching devices and the dead time effect in switching signals influence the MMC operation. In Fig. 2 the non-ideal parameters are represented by equivalent resistances r_{pU}, r_{pL} and voltage sources v_{pU} and v_{pL}. All those parameters are not constant and can be presented as a function of the modulating signals n_{U} and n_{L} and arm current direction. The r_{pU} can be written as (18).

$$r_{\text{pU}} = \begin{cases} n\left[n_{\text{U}}\left(r_{\text{D}} + R_{\text{ESR}}\right) + \left(1 - n_{\text{U}}\right) r_{\text{T}}\right] & \text{for} \quad i_{\text{arm}} > 0, \\ n\left[n_{\text{U}}\left(r_{\text{T}} + R_{\text{ESR}}\right) + \left(1 - n_{\text{U}}\right) r_{\text{D}}\right] & \text{for} \quad i_{\text{arm}} < 0, \end{cases} \tag{18}$$

where n is the number of submodules in a single arm, r_T and r_D are on-state resistances of transistor and diode respectively, R_{ESR} is the equivalent series resistance of a single submodule capacitor C_{SM}. The transistor and diode resistances can be comparable; they can therefore be equal to on-state resistance r_{on}, $r_T \approx r_D = r_{on}$, which in return simplifies Eqs. (18) to (19).

$$r_{pU} = n\left(n_U R_{ESR} + r_{on}\right). \tag{19}$$

A similar simplification can be made for r_{pL} as in (20).

$$r_{pL} = n\left(n_L R_{ESR} + r_{on}\right). \tag{20}$$

Both non-ideal parameter resistances $r_{pU} r_{pL}$ are time varying due to n_U and n_L, which are given in (13).

Voltage sources v_{pU} and v_{pL} depend on transistor and diode threshold on-state voltages V_{T0}, V_{F0} according to (21) and (22).

$$v_{pU} = \begin{cases} n\left[n_U V_{F0} + \left(1 - n_U\right) V_{T0}\right] & \text{for} \quad i_{armU} > 0, \\ -n\left[n_U V_{T0} + \left(1 - n_U\right) V_{F0}\right] & \text{for} \quad i_{armU} < 0, \end{cases} \tag{21}$$

$$v_{pL} = \begin{cases} n\left[n_L V_{F0} + \left(1 - n_L\right) V_{T0}\right] & \text{for} \quad i_{armL} > 0, \\ -n\left[n_L V_{T0} + \left(1 - n_L\right) V_{F0}\right] & \text{for} \quad i_{armL} < 0. \end{cases} \tag{22}$$

The dependence of voltage sources v_{pU} and v_{pL} on the direction of the arm current complicates the analysis of the influence of such voltage sources on converter operation. Here in this paper the analysis of non-ideal parameters is limited to presenting their major influence. This can be done by using one of the state equations (5), which is now rewritten to (23) – including the non-ideal parameters. The non-ideal parameters change both equations (3) too – this is due to the existence of series equivalent resistance in all capacitors. However this impact is not discussed in the paper.

$$\frac{\mathrm{d}}{\mathrm{d}t} i_{diff} = \frac{-2R_{arm} - r_{pU} - r_{pL}}{2L_{arm}} i_{diff} - \frac{v_{armU} + v_{armL}}{2L_{arm}} + \frac{V_{dc}}{2L_{arm}} - \frac{v_{pU} + v_{pL}}{2L_{arm}}, \tag{23}$$

where arm voltages can now be expressed by (24)

$$\begin{aligned} v_{armU} &= \frac{V_{dc}}{2} - m_a \frac{V_{dc}}{2} \sin\left(\omega t - \psi\right) + v_{disU}, \\ v_{armL} &= \frac{V_{dc}}{2} + m_a \frac{V_{dc}}{2} \sin\left(\omega t - \psi\right) + v_{disL} \end{aligned} \tag{24}$$

and voltages v_{disU} and v_{disL} are the discrepancy arm voltage components – resultant from the existence of ripples in capacitor voltages. The exact analytical form of discrepancy voltages is not the subject of this paper, but can be determined only after determining the analytical form of the difference current. After substituting (24) for (23) the derivative of the difference current can be expressed as

$$\frac{\mathrm{d}}{\mathrm{d}t} i_{diff} = -\frac{2R_{arm} + r_{pU} + r_{pL}}{2L_{arm}} i_{diff} - \frac{v_{disU} + v_{disL}}{2L_{arm}} - \frac{v_{pU} + v_{pL}}{2L_{arm}}. \tag{25}$$

It can be seen from (25) that the effect of the non-ideal parameters on the difference current is similar to the effect of arm resistance and discrepancy arm voltages. This effect cannot be neglected if voltages v_{pU} and v_{pL} are comparable with voltages v_{disU} and v_{disL} or resistances r_{pU}, r_{pL} are comparable with R_{arm}.

5. Simulation results

In this section the operation of a detailed simulation model of 5-submodule MMC is presented. The results of MMC operation are shown for the converter with ideal parameters.

Among many PWM strategies, which can be used in the MMC, the triangle carrier based PWM technique is typically applicable. This strategy can differ in the phase shift between triangular carrier signals S_N, which are compared with modulating signals n_U, n_L. In the modulation strategy of five-submodule MMC, five carrier signals are used in each converter arm. In the paper the two following PWM strategies are analyzed:

a) the method with zero degree upper and lower arm carrier phase shift, $\gamma = 0°$, which is very similar to the phase disposition PWM method (PD PWM) – the method commonly used in other multilevel converters. Here, all 5 upper arm carriers, S_{NU} and all 5 lower arm carriers, S_{NL}, are in phase as per Fig. 12,
b) the method with zero degree upper and 180° lower arm carrier phase-shift, $\gamma = 180°$ which is similar to the method known as phase opposition disposition PWM (POD PWM). Here, all 5 upper arm carriers S_{NU} are out of phase with those in the lower arm, S_{NL}, as per Fig. 14.

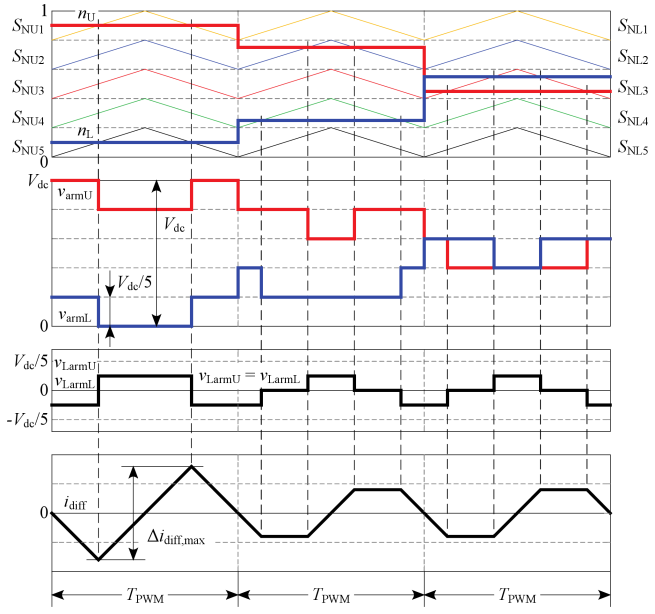

Fig. 12. Construction of the MMC arm voltages with the direct modulation method and the phase disposition PWM strategy with a carrier phase-shift angle $\gamma = 0°$

Both modulation strategies are based on the direct modulation method with modulating signals n_U, n_L given as per (13).

In Fig. 12 arm voltages v_{armU} and v_{armL} during three switching periods T_{PWM} are presented. In this case the carrier phase angles are the same ($\gamma = 0°$), therefore switchings occurs in both arm voltage waveforms in the same direction – the first one with a falling slope (when all carriers increase), and the second one with a rising slope (when all carriers decrease). In such a case, the sum of both arm voltages $v_{\text{armU}} + v_{\text{armL}}$ is not equal to V_{dc} but is either $V_{\text{dc}} + V_{\text{dc}}/n$ or $V_{\text{dc}} - V_{\text{dc}}/n$ (assuming a constant sum of capacitor voltages $v_{\text{CU}} = v_{CL} = V_{\text{dc}}$). The difference between the arm voltages sum, $v_{\text{armU}} + v_{\text{armL}}$, and dc circuit voltage, V_{dc}, equals to $+/- V_{\text{dc}}/n$ and occurs across both arm inductors. Voltages across the arm inductances (v_{LarmU} and v_{LarmL}) are the same, thus $v_{\text{LarmU}} = v_{\text{LarmL}} = +/- V_{\text{dc}}/(2n)$ – Fig. 12.

Arm voltages lead to the occurrence of relatively high difference current ripples (Fig. 12). The highest ripples exist in periods when modulating signals are in the middle of each carrier signal (e.g. first switching period T_{PWM} in Fig. 12). In such a case the maximum difference current ripple $\Delta i_{\text{diff,max}}$ is

$$\Delta i_{\text{diff,max}} = \frac{1}{L_{\text{arm}}} \frac{V_{\text{dc}}}{2n} \frac{T_{\text{PWM}}}{2}. \tag{26}$$

The maximum difference current ripple $\Delta i_{\text{diff,max}}$ is relatively high, for instance when $V_{\text{dc}} = 5000$ V, $n = 5$ and $L_{\text{arm}} = 750$ μH, $T_{\text{PWM}} = 200$ μs ($1/T_{\text{PWM}} = 5$ kHz), (26) returns $\Delta i_{\text{diff,max}} = 66.7$ A. This particular current ripple compared to the output current amplitude $I_{\text{V}} = 40$ A is relatively high.

Figure 13 presents waveforms in the MMC operating with a zero degree phase-shift in all carriers S_{NU} and S_{NL}, $\gamma = 0°$. These results are obtained from the three-phase simulation model of the converter, which has been developed in Matlab/Simulink. Converter parameters are listed in Table 1 with the switching frequency equal to $f_{PWM} = 5$ kHz. In Fig. 13 it can be seen that in the difference current (and in both arm currents) relatively high ripples occur, the maximum value of which is equal to the value from (26). The output voltage e_{V}, (as in Fig. 2) consists of 11 levels maximally. Such a number comes from the achievable values of the voltage, $v_{\text{armL}} - v_{\text{armU}}$ (9), where six levels are present (n+1 per single n-submodule MMC arm) in each arm voltage.

Maximum ripples in i_{armU}, i_{armL} are equal to $\Delta i_{\text{diff,max}} = 66.7$ A. Depending on the phase-shift angle between carrier signals in different phases of the converter, the ripples in the dc-circuit current i_{dc} can be even higher than $\Delta i_{\text{diff,max}}$. The capacitor voltage ripple of a single capacitor (peak-to-peak value) is approximately equal to 90 V, thus the ripple in arm capacitor voltage is $\Delta V_{\text{C}} = 450$ V. This value is higher than the value obtained for the averaged model of the converter (where $\Delta V_C = 406$ V). Such a difference can be explained by a higher ripple in the difference current and the operation of the capacitor voltage balancing circuit.

The occurrence of such high ripples in the arm currents practically disqualifies this modulation method ($\gamma = 0°$). Therefore, the second PWM strategy, where carrier signals are with opposite phase angles, is chosen. In this method the upper arm carriers are $\gamma = 180°$ away from the lower arm carriers. Signals from the PWM modulator together with voltage and current waveforms are shown in Figs. 14 and 15.

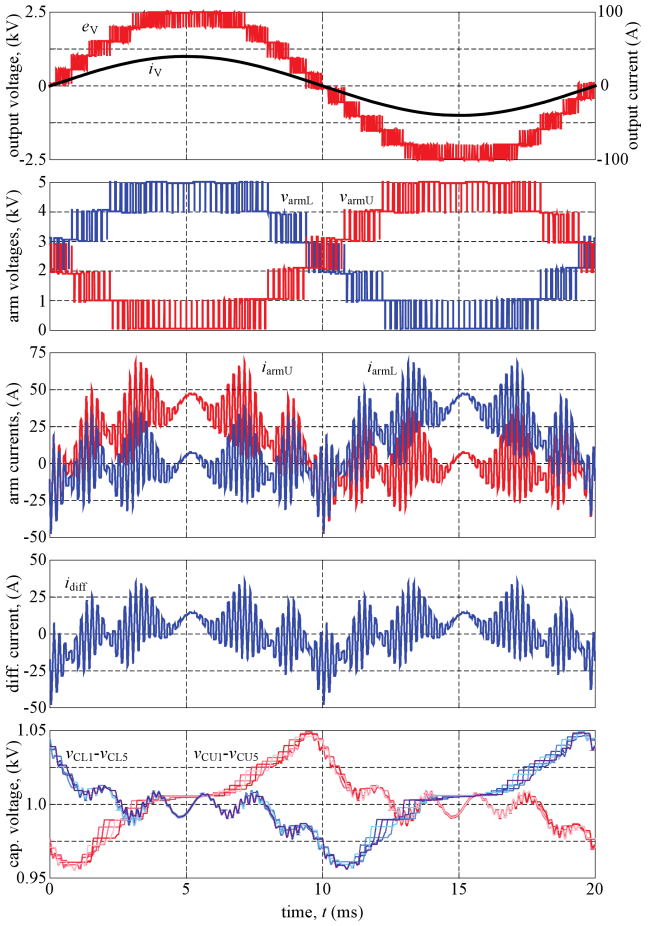

Fig. 13. Current and voltage waveforms of the MMC operating with the direct modulation method and zero degree carrier phase shift, $\gamma = 0°$

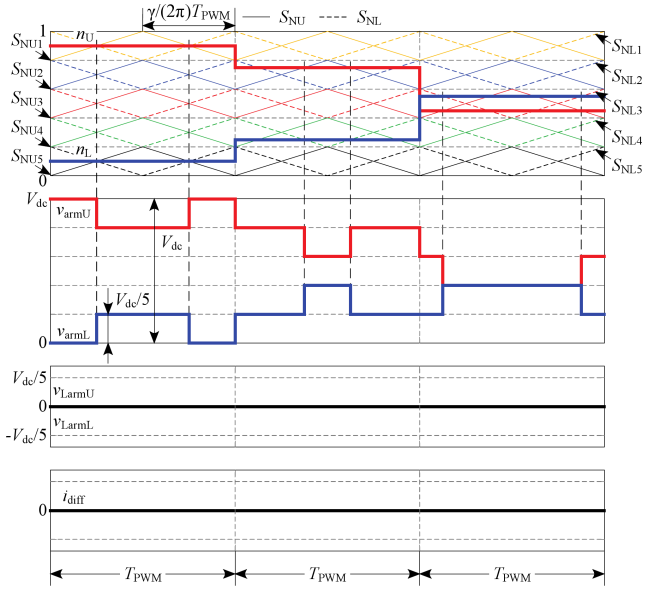

Fig. 14. Construction of the MMC arm voltages under the direct modulation method and the PWM strategy where the upper arm carriers are opposite to carriers from the lower arm, $\gamma = 180°$

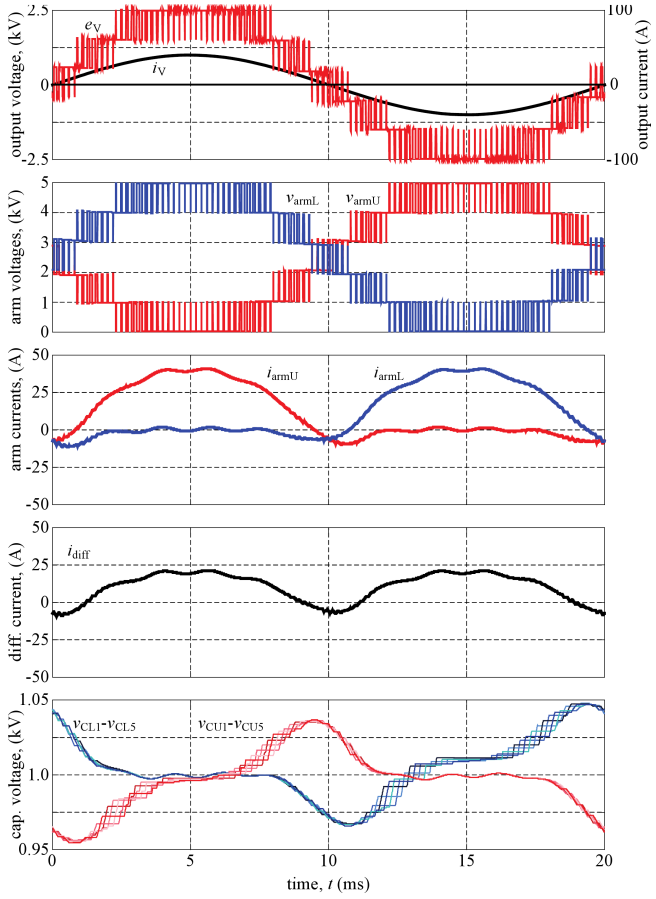

Fig. 15. Current and voltage waveforms of the MMC with the direct modulation method and the PWM strategy, where the upper arm carriers are opposite to carriers from the lower arm, $\gamma = 180°$

From Fig. 14 one can see that due to the complementary shape of the v_{armU} and v_{armL} their sum is equal to V_{dc} ($v_{armU} + v_{armL} = V_{dc}$). This leads to reduction of the ripple in the difference current because both arm inductor voltages equal zero $v_{LarmU} = v_{LarmL} = 0$. In practice the capacitor voltage ripple and other non-ideal parameters of the converter can cause small ripples during the switching period T_{PWM}. However, they are relatively small.

In the example from Fig. 15 voltage and current waveforms are obtained from the three-phase converter detailed model which has been developed in Matlab/Simulink. The parameters of such a converter are the same as in Table 1 and the phase-shift angle of carrier signal is $\gamma = 180°$. The differences existing between waveforms in Figs. 13 and 15 are as follows:

- the output voltage e_V has six voltage levels rather than 11 in the first case,
- no significantly high harmonic ripple exists in arm currents i_{armU}, i_{armL},
- the difference current consists of harmonic components which are predicted in the averaged model. The current waveform is similar to the one in Fig. 3. The harmonic spectrum of this current is depicted in Fig. 5 (point A),
- ripples in the arm capacitor voltages, when summed up, are equal to $\Delta V_C = 5 \times 80$ V $= 400$ V – this is similar to the value presented in Figs. 9–11 at point A.

The simulation results presented in Fig. 15 prove the correctness of the analyses based on the averaged mathematical model of the MMC.

6. Simulation model performance

This paragraph is devoted to a comparison of six simulation models of the modular multilevel converter, the results of which have been presented in this paper. These models have been developed in Matlab/Simulink and GeckoCIRCUITS and they are as follows:

- averaged model of a single-phase MMC (1AM or 1AG),
- averaged model of a three-phase MMC (3AM or 3AG),
- detailed model of a three-phase MMC (3DM or 3DG),

where letters M and G correspond to Matlab/Simulink and GeckoCIRCUITS.

All the results obtained from the models implemented in GeckoCIRCUITS are similar to those obtained by using Matlab/Simulink models. However, the computational time of all models' simulations differ between these two simulators. To compare all the developed simulation models, the computational time of simulation is chosen as a criterion.

All the simulation models, the parameters of which are the same as in Table 1, are executed with the simulation step equal to 1 μs (1e-6) for the simulation time ranging from 0 to 1.5 seconds. Models in Matlab/Simulink are executed using a discrete fixed-step solver, guaranteeing the smallest computational time among other available solvers. GeckoCIRCUITS models are executed with a Backward Euler solver, which guarantees accurate simulation results.

Each model has been simulated for 20 iterations to find a mean value of computational time. This method offers more reliable results, which can be next used to compare different models – Fig. 16. Computational times of all the models have been obtained by using personal computer with a quad-core microprocessor Intel® Core™ i7-3630QM @ 2.4 GHz, whose number of floating point computations per second is 1724 MFLOPS for a single core and 6650 MFLOPS for all four cores.

The simulation computational time strongly depends on the number of variables observed in the models. Therefore, in all the models only a limited number of variables are observed and they are the same as presented in Figs. 3, 13 and 15. For three-phase models only one converter phase is measured. For increasing the computational time, the simulation results are transferred to memory rather than the computer display unit.

It should be noted that the results presented in Fig. 16 cannot be directly transferred to other computers. However, there is a close relationship between computer performance, measured in MFLOPS, and simulation computational time.

In Fig. 16 it can be clearly seen that averaged models are computed much faster than detailed ones. For Matlab/Simulink three-phase models the averaged one is comput-

ed more than 14.6 times faster and for GeckoCIRCUIT this relationship is even higher and equals to 21.6. The simulation computational time can be further decreased by simulating merely a single-phase converter, which gives similar results in the case of supplying the converter from an ideal dc voltage source.

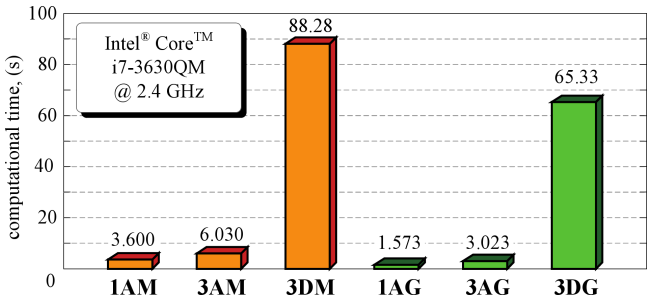

Fig. 16. Simulation computational time for averaged (A) and detailed (D) models of a single-phase (1) or three-phase (3) MMC implemented in Matlab/Simulink (M) or GeckoCIRCUITS (G)

The analyzed models developed in Matlab/Simulink or GeckoCIRCUITS cannot be easily compared with each other because the computational time strongly relies on the number of variables being observed in the simulation. And this relationship is different in Matlab/Simulink, which allows observing more variables without increasing computational time as drastically as in the case of GeckoCIRCUITS. The authors are aware of the fact that all the presented models can be computed by using many different simulators or computational methods, which allow achieving even faster computational times. It is, however, true that averaged models are computed much faster than detailed ones.

A shorter computational time allows performing different analyses on converter operation. They include a power loss analysis (without switching losses due to a lack of switchings in the model) [12]; the second important analysis can be used for converter parameter selection [5].

On the other hand, some effects can be modelled only by means of a detailed model with switches. These include dc voltage balancing, dead time effects or the effect of non-ideal parameters on converter control. It is up to the user which model is chosen to observe a required feature of the converter.

7. Conclusions

The influence of two main MMC parameters, arm resistance and arm capacitance, on converter operation has been investigated in the paper. This influence is strong, particularly on the circulating current and capacitor voltages ripple. The analysis was confined to 5 kV DC circuit voltage, 40 A of output current amplitude and 0.75 mH of arm inductance with a unity modulation index. The direct modulation strategy was assumed. In the analysis variable parameters are within the range usually quoted in the literature of the subject as representative.

The main influence of the presented parameters is observed as resonances in circulating currents and capacitor voltages. The arm parameters, resistance, capacitance and also inductance should be carefully selected in order to avoid resonances. This needs further investigation, where circulating currents and capacitor voltage ripple are minimized within the range constrained by a given application.

The presented results have been obtained using two computer models, the averaged and the detailed one. The first one is relatively simple and demands less computational time. This model does not reflect all of the operational details, like switching. However, it allows one to carry out an analysis in a much broader range. The model can be applied for an introductory analysis, the results of which could be used by the detailed model. The second detailed model embraces transistor switching and PWM strategy, which significantly influences MMC behaviours. The price of a more precise picture of the converter operation is the much larger computational time.

Both models can be extended by non-ideal parameters like transistor or diode, threshold voltage and its dynamical resistance, to name just a few.

The models are not dependent on the selected modulation strategy (direct, open loop control).

In conclusion, the presented analysis is recommended for MMC designing.

Acknowledgements. This paper has been prepared under a project financed by ABB Corporate Research Center in Kraków, Poland.

REFERENCES

[1] A. Lesnicar and R. Marquardt, "An innovative modular multilevel converter topology suitable for a wide power range", *IEEE Conf. Power Tech.* 3, 1–6 (2003).

[2] A. Antonopoulos, L. Ängquist, and H.-P. Nee, "On dynamics and voltage control of the modular multilevel converter", *Conf. on Power Electronics and Applications, EPE 2009* 1, 1–10 (2009).

[3] A. Antonopoulos, K. Ilves, L. Ängquist, and H.-P. Nee, "On interaction between internal converter dynamics and current control of high-performance high-power ac motor drives with modular multilevel converters", *IEEE Energy Conversion Congress and Exposition ECCE* 1, 4293–4298 (2010).

[4] J. Kolb, F. Kammerer, and M. Braun, "Straight forward vector control of the modular multilevel converter for feeding three-phase machines over their complete frequency range", *IEEE Industrial Electronics Society Conf. IECON 2011* 1, 1596–1601 (2011).

[5] M. Zygmanowski, B. Grzesik, and R. Nalepa, "Capacitance and inductance selection of the modular multilevel converter", *Conf. on Power Electronics and Applications, EPE* 1, 1–10 (2013).

[6] A. Hillers and J. Biela, "Optimal design of the modular multilevel converter for an energy storage system based on split batteries", *Conf. on Power Electronics and Applications, EPE 2013* 1, 1–11 (2013).

[7] D. Siemaszko, A. Antonopoulos, K. Ilves, M. Vasiladiotis, L. Ängquist, and H.-P. Nee, "Evaluation of control and modulation methods for modular multilevel converters", *Int. Power Electronics Conf. IPEC* 1, 746–753 (2010).

[8] S. Rohner, S. Bernet, M. Hiller, and R. Sommer, "Analysis and simulation of a 6 kV, 6 MVA modular multilevel converter", *IEEE Industrial Electronics Society Conf.* 1, 225–230 (2009).

[9] L. Ängquist, A. Antonopoulos, D. Siemaszko, K. Ilves, M. Vasiladiotis, and H.-P. Nee, "Inner control of modular multilevel converters - an approach using open-loop estimation of stored energy", *Int. Power Electronics Conf. IPEC 2010* 1, 1579–1585 (2010).

[10] Qingrui Tu, Zheng Xu, and Lie Xu, "Reduced switching-frequency modulation and circulating current suppression for modular multilevel converter", *IEEE Trans. Power Delivery* 26 (3), 2009–2017 (2012).

[11] M.A. Pérez, J. Rodríguez, E.J. Fuentes, and F. Kammerer, "Predictive control of ac–ac modular multilevel converters", *IEEE Trans. Ind. Electr.* 59 (7), 2832–2839 (2012).

[12] M. Zygmanowski, B. Grzesik, M. Fulczyk, and R. Nalepa, "Analytical and numerical power loss analysis in modular multilevel converter", *IEEE Industrial Electronics Society Conf. IECON* 1, 465–470 (2011).

[13] K. Ilves, A. Antonopoulos, S. Norrga, and H.P. Nee, "Steady-state analysis of interaction between harmonic components of arm and line quantities of modular multilevel converters", *IEEE Trans. Power Electronics* 27 (1), 57–68 (2012).

[14] S. Rohner, S. Bernet, M. Hiller, and R. Sommer, "Modulation, losses, and semiconductor requirements of modular multilevel converters", *IEEE Trans. Ind. Electr.* 57 (8), 2633–2642 (2010).